Environmental Science & Technology

Article

Cite This: Environ. Sci. Technol. 2018, 52, 11591−11600

pubs.acs.org/est

Field-Induced Redistribution of Surfactants at the Oil/Water Interface Reduces Membrane Fouling on Electrically Conducting Carbon Nanotube UF Membranes

Xiaobo Zhu,[†] Alexander V. Dudchenko,[‡] Chia Miang Khor,[†] Xin He,[§] Guy Z. Ramon,[∥] and David Jassby*[,†]

[†]Department of Civil and Environmental Engineering, University of California, Los Angeles, Los Angeles, California 90095, United States

[‡]Department of Civil and Environmental Engineering, Carnegie Mellon University, Pittsburgh, Pennsylvania 15213, United States

[§]The College of Environmental Science and Engineering, Nankai University, Tianjin, China

[∥]Department of Civil and Environmental Engineering, Technion − Israel Institute of Technology, Haifa, Israel

Supporting Information

ABSTRACT: Membrane-based treatment of oily wastewater remains a significant challenge, particularly under high salinity conditions. The main difficulty associated with this separation process is membrane fouling, mostly caused by wetting and coalescence of emulsified oil droplets on the membrane surface. In this study, electrically conducting carbon nanotube-based ultrafiltration membranes were used to treat an emulsified oil suspension at ionic strengths as high as 100 mM. By tuning the electrical potential applied to the membrane surface, we demonstrate how fouling can be dramatically reduced, even under high salinity conditions. Permeate water quality is shown to improve upon application of a negative potential. Using optical microscopy, we observed dramatic changes in the shape of oil droplets at the membrane/water interface in response to the applied electric potential; this change is associated with a redistribution of charged surfactant molecules at the oil/water interface in response to the external electric field. Specifically, using the membrane as a cathode repels surfactant molecules away from the oil/membrane interface, while anodic conditions lead to increased surfactant concentrations. We speculate that this change in surfactant molecule distribution is responsible for changes in the surface tension of oil droplets at the membrane/water interface, which results in a decrease in oil coalescence and subsequent fouling. The membranes used in this study offer an attractive treatment option when separating emulsified oil from water under high salinity conditions.

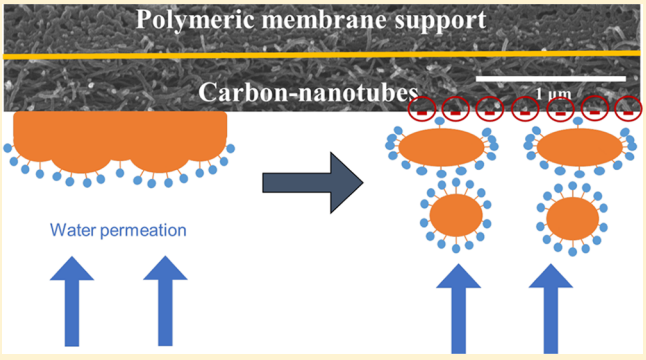

1. INTRODUCTION

Oily wastewater is generated from a wide range of industrial activities.[1−4] For example, hydraulic fracturing of geologic formations in the pursuit of oil and gas generates large volumes of produced water which can contain large amounts of emulsified oil.[5−7] In the United States, there are approximately 60 million barrels of produced water generated daily.[8] The disposal of this water often requires transportation to remote deep-well injection sites, dramatically increasing the cost of produced water treatment.[9,10] Another example is the treatment of oil-contaminated bilge water.[11] Traditional gravity-based separation methods are effective at removing large and unstable oil droplets (>10 μm).[12] However, emulsified oil drops with sizes <10 μm are not easily removed by gravity.[3] Thus, the treatment of contaminated bilge water has been particularly challenging for ship operators. The effective separation of emulsified oil from water would be a step toward the discharge of this contaminated water directly to receiving water bodies.[13]

Membrane separation has been demonstrated to be an effective method for emulsified oil/water separation, with a variety of membrane processes explored for this purpose. Hydrophilic polysulfone ultrafiltration (UF) membranes can reject over 90% of well stabilized droplets;[14] hydrophobic polyvinylidene difluoride membranes allow the hydrophobic oil phase rather than the water to pass through, increasing energy efficiency due to the smaller fraction of oil than water in an emulsion;[15] forward osmosis membranes demonstrated high water flux and oil rejection;[16,17] thermally driven membrane distillation processes

Received: May 14, 2018
Revised: September 12, 2018
Accepted: September 17, 2018
Published: September 17, 2018

DOI: 10.1021/acs.est.8b02578
Environ. Sci. Technol. 2018, 52, 11591−11600

were shown to be capable of purifying produced water with high salinity and oil content;[18−21] inorganic membranes, such as glass fiber and copper meshes, decorated with hydrophilic substances to become superhydrophilic or superoleophobic, achieved high rejection rates across a broad pH range (1−13).[22,23] Due to the relatively large size of emulsified oil drops in water (typically >1 μm), low pressure membrane processes (such as UF) are highly effective at removing these oil drops from water;[24] the low energy consumption associated with these membranes make them particularly attractive for the treatment of oily wastewater.[25]

While membrane-based separation processes are highly effective for oil/water separations, membranes suffer from fouling, which reduces their performance and requires periodic cleaning.[26−28] During the treatment of oil emulsion in water, the emulsified oil droplets accumulate on the membrane surface, where they are subject to various forces. While some forces limit membrane fouling (electrostatic repulsive forces between neighboring emulsified oil drops, and between drops and the membrane surface, and lifting forces caused by the tangential flow of water across the membrane surface), other forces promote membrane fouling (drag forces generated by water flowing through the accumulated oil drop layer, and van der Waals forces). In addition to these forces, the dielectrophoretic force has been used for particle separation due to a net repulsive force resulting from a nonuniform electric field.[29,30] When the fouling forces dominate, membrane fouling can result from oil drop coalescence and/or from membrane wetting (i.e., when the oil is absorbed by the membrane).[24,31,32]

Droplet interfacial properties play an important role in droplet coalescence and membrane surface wetting. In general, an oil-in-water emulsion is stabilized by a layer of surfactant molecules that break strong hydrogen bonds between water molecules along the oil/water interface. This lowers the interfacial tension between oil and water, and also forms a charged droplet surface that can repel one droplet from another, preventing neighboring oil drops from coalescing.[33]

The interfacial tension at the oil/water interface is dependent on the solution ionic strength, with higher salt concentrations leading to lower interfacial tensions;[34,35] at elevated ionic strengths, screening of the charged surfactant head, as well as possibly a "salting-out" effect allows for higher surfactant packing density at the oil/water interface, leading to enhanced steric hindrance that prevents droplet coalescence.[35]

Carbon nanotube (CNT)-based electrically conducting membranes have shown great promise in preventing numerous types of membrane fouling, such as organic fouling,[36,37] biofilm formation,[38,39] and inorganic salt scaling.[40,41] The goal of study paper is to investigate the fouling behavior of electrically charged membranes during the treatment of well-stabilized oil emulsions under high salinity conditions. Different electrical potentials, as both AC and DC, were applied on CNT membranes at various fluxes and ionic strengths. Membrane properties, droplet characteristics and permeate chemistry were investigated accordingly.

2. MATERIALS AND METHODS

2.1. Membranes and Chemicals. Commercially available Poly(ether sulfone) (PES) UF membranes with a molecular weight cut off of 20 kDa (Synder Filtation, CA) were used as the conducting membrane substrate in all filtration experiments. Hexadecane (99.8%, Fisher Scientific), sodium chloride (NaCl, 99.5%, Sigma-Aldrich), dodecylbenzenesulfonate sodium salt (DDBS, technical grade, Sigma-Aldrich) and carboxylic groups functionalized multiwalled CNTs (99 wt %, Cheap Tubes, outer diameter of 13−18 nm, tube length of 3−30 μm, and COOH content of 7.0%) were used as received.

2.2. Membrane Fabrication and Characterization. Electrically conducting membranes were fabricated based on a previously published method.[41] In short, a solution containing 0.1 g/L CNTs and 1 g/L DDBS was sonicated for 30 min using a horn sonicator (450 Digital Sonifier, Branson), followed by centrifugation at 11 000 rcf (Avanti J-E Centrifuge, Beckman Coulter) to remove undispersed particulates. After this, 75 mL of the CNT suspension were pressure-deposited on the PES membrane support using a dead-end filtration cell at 60 psi. A uniform CNT layer with a thickness of approximately 2 μm was formed. Membrane surface morphology, expressed as the root-mean-square of roughness, was characterized by atomic force microscopy (AFM) in tapping mode (scan rate: 0.2 Hz), based on a grid size of 10 μm × 10 μm (MFP-3D Classic, Asylum). A 4-point conductivity probe was used to characterize the membrane sheet resistance (MCP-T610, Mitsubishi). Membrane surface potentials vs a Ag/AgCl reference were measured using a 3-electrode configuration (with a Pt-coated Ti plate as a counter electrode) connected to a potentiostat (Supporting Information (SI) Figure S1, 600E Potentialstat, CH Instruments).

2.3. Emulsion Preparation and Characterization. Oil emulsions were prepared by homogenizing 5 g/L hexadecane, 100 ppm DDBS, and 0, 10, or 100 mM NaCl in 1.5 L deionized (DI) water at 4000 rpm for 2 min (IKA T50 homogenizer, Cole-Parmer). Size and charge of the oil droplets were characterized by an optical microscope (Axioskop 2 plus, Zeiss) and a zeta potential analyzer (ZetaPALS, Brookhaven Instruments Corporation), respectively. Droplet size distributions were calculated based on the diameters of more than 100 drops, using image analysis software (ImageJ).

2.4. Contact Angle and Interfacial Tension Measurement. Hexadecane was injected into 100 ppm DDBS solution with 0 and 100 mM NaCl electrolyte. The underwater contact angle and interfacial tension (of the oil/water interface) were measured using a contact angle goniometer equipped with proprietary image analysis software (model 250, Rame-hart).

2.5. Membrane Filtration Process. For the filtration experiments, electrically conducting membranes were placed into a custom-built cross-flow filtration cell (active membrane area of 10 cm × 4 cm, with a channel height of 3.8 mm) designed to accommodate electrically conducting membranes.[37] A Pt-coated Ti plate, with dimensions identical to active membrane surface area, was placed 3.8 mm above the membrane surface and used as a counter-electrode. Water was circulated through the flow cell using a diaphragm pump (Hydra-Cell, MN), at a flow rate of 1 L/min, which translates into a cross-flow velocity of 11 cm/s. Prior to studying membrane surface fouling, CNT membranes were prewetted with methanol, then compressed at 100 psi until water flux stabilized at between 60 and 90 $L \cdot m^{-2} \cdot h^{-1}$ (LMH). Membrane fouling was investigated using a customized filtration system operating in constant flux mode, with the flux maintained at 10, 20, and 30 LMH.[31,42] For each experimental condition, the filtration process was operated for 2 h in three cycles, with a 5 min backwashing step and a 5 min cross-flushing step (together termed "hydraulic cleaning") using the feed solution at 0 psi between each cycle. Membrane fouling was expressed as an increase in the required pressure needed to maintain the

DOI: 10.1021/acs.est.8b02578
Environ. Sci. Technol. 2018, 52, 11591−11600

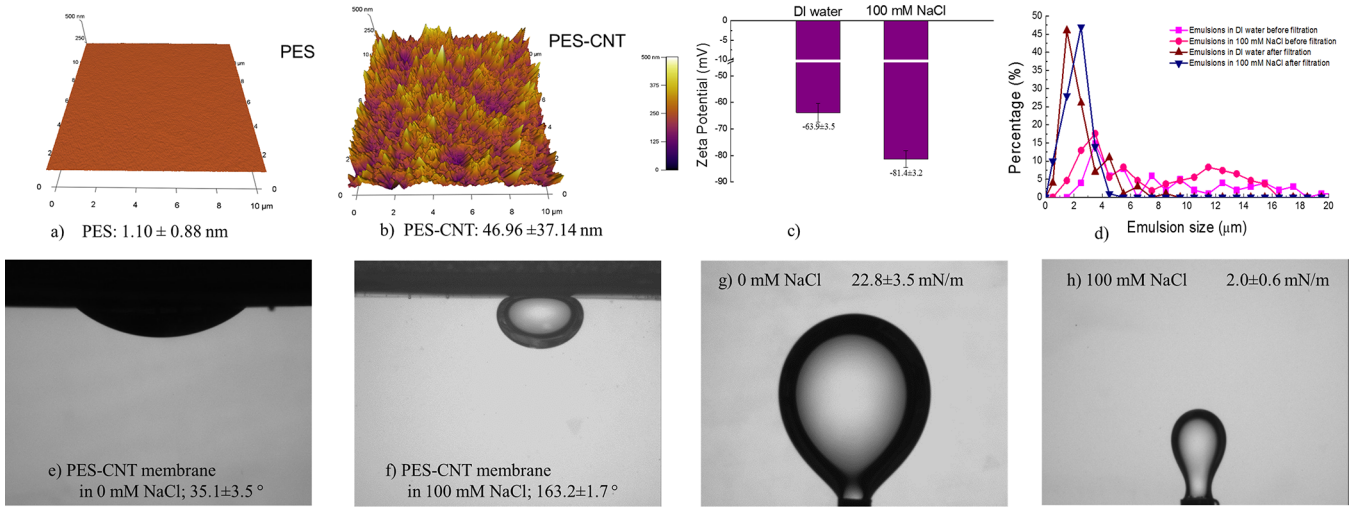

Figure 1. Membrane and droplet characterization: Membrane surface morphology and surface roughness of (a) PES membrane and (b) PES-CNT membrane; (c) droplet zeta potentials under different ionic strength conditions; (d) droplet size distribution in DI water and 100 mM NaCl solutions; contact angle of DDBS-stabilized oil droplets on CNT membranes in (e) DI water, and (f) 100 mM NaCl solution; interfacial tension of DDBS stabilized oil droplet in (g) DI water, and (h) 100 mM NaCl solution.

constant flux. Electrical potentials of 0 V, 2.5 V_{dc}, 5 V_{dc}, and 2.5 V_{ac} @ 1 Hz were applied to the membrane/counter electrode during the entire filtration process using an arbitrary waveform generator (DG1022, Rigol), with the membrane always functioning as the cathode (i.e., the membrane was negatively charged) when DC potentials were applied; for the 2.5 V_{ac} conditions, a Sine waveform was used (i.e., ± 2.5 V). Two ionic strength conditions, 0 and 100 mM NaCl, were tested. All experiments were done in triplicate.

2.6. Permeate Water Quality Analysis. Permeate water quality was evaluated by measuring the total organic carbon (TOC) using a TOC analyzer (TOC, 1030W, O.I. Analytical). The surfactant concentration was measured using the formation of the ionic pair between methylene blue and the anionic surfactant.[43]

3. RESULTS AND DISCUSSION

3.1. Membrane and Emulsion Characterization. Membrane surface contours, as measured by AFM in tapping mode, were used to evaluate surface roughness (Figure 1a, 1b). The pristine PES membranes have a very smooth surface with a roughness of 1.1 ± 0.8 nm (Figure 1a). The deposition of the CNT layer increased surface roughness to 47 ± 37 nm (Figure 1b). The sheet resistance of CNT membranes was measured to be 176.1 ± 9.3 Ω/□, which translates into a conductivity of 2839.3 ± 149.9 S/m. The electrical resistance of the dry membrane inside the flow cell was 289.6 ± 20.1 Ω (measured across a 10 cm flow channel); once water was introduced into the cell, the resistance increased to 412.1 ± 20.4 Ω, and stayed constant throughout the experiment. The increase in resistance is likely caused by slight swelling of the CNT layer, which would increase the contact resistance between neighboring CNTs. Furthermore, the fact that the electrical resistance did not change over the course of the experiments indicates that the CNTs formed a stable layer that did not lose CNTs. Our previous study indicated that the pore-size of these membranes was approximately 125 nm, which agrees with findings that state that the pore sizes of a fiber network range between 6 and 8× the fiber diameter.[44]

The pH of the emulsion was determined to be 6.01 ± 0.50 and 5.72 ± 0.30 in the 0 and 100 mM NaCl solutions, respectively. Zeta potentials of oil droplets in DI water and in 100 mM NaCl solution are reported in Figure 1c. As can be seen, the zeta potential increased from −63.9 ± 3.5 to −81.4 ± 3.2 mV with the addition of NaCl. Using the Gibbs adsorption isotherm (SI Section SI 3), we calculated that the surfactant concentration at the oil/water interface increased from 6.268 × 10^{-7} mol/m^2 in 0 mM NaCl to 3.092 × 10^{-6} mol/m^2 in 100 mM NaCl (SI Table S2, Figure S2). This increase is a result of enhanced charge screening of the charged sulfonate groups of the surfactant molecules at higher electrolyte concentrations.[45,46] This increase in charge density can lead to the observed enhanced zeta potential at higher ionic strengths (Figure 1c). While an increase in solution temperature leads to increased measured mobility, we determined that no significant temperature differences occurred under the 0 mM and 100 mM conditions (due to resistive heating in the solution), and thus, the zeta potential measurements were reflective of enhanced surface charge density at higher ionic strengths. The increased adsorption of surfactant molecules at the oil/water interface is a result of decreased electrostatic repulsion between neighboring adsorbed surfactant molecules, which allows for higher surfactant concentrations at the oil/water interface, Interestingly, there was a dramatic reduction in droplet size after the membrane filtration process (in the retentate), with the size of emulsified oil drops decreasing from 14.9 ± 11.0 before the experiment to 2.4 ± 1.5 μm after the experiment in DI water, and from 7.5 ± 4.5 to 2.2 ± 0.9 μm in 100 Mm NaCl (SI Table S1, Figure 1d). This was likely caused by shear forces in the fluid channel and pump head, which sheared larger drops into progressively smaller droplets.[47] Oil droplets in both DI water and NaCl solutions have similar sizes after filtration, which suggests that droplet size is controlled by the shear rate in the membrane filtration system. Figure 1d demonstrates the wide size distribution of freshly made emulsions, ranging from 0 to 40 μm, and the far narrower distribution following the filtration experiments. We believe that the relevant emulsion sizes during these experiments are 2.4 ± 1.5 μm in DI water, and 2.2 ± 0.9 μm in 100 mM NaCl.

3.2. Contact Angle and Interfacial Tension. Contact angle and interfacial tension measurements are summarized in

DOI: 10.1021/acs.est.8b02578
Environ. Sci. Technol. 2018, 52, 11591−11600

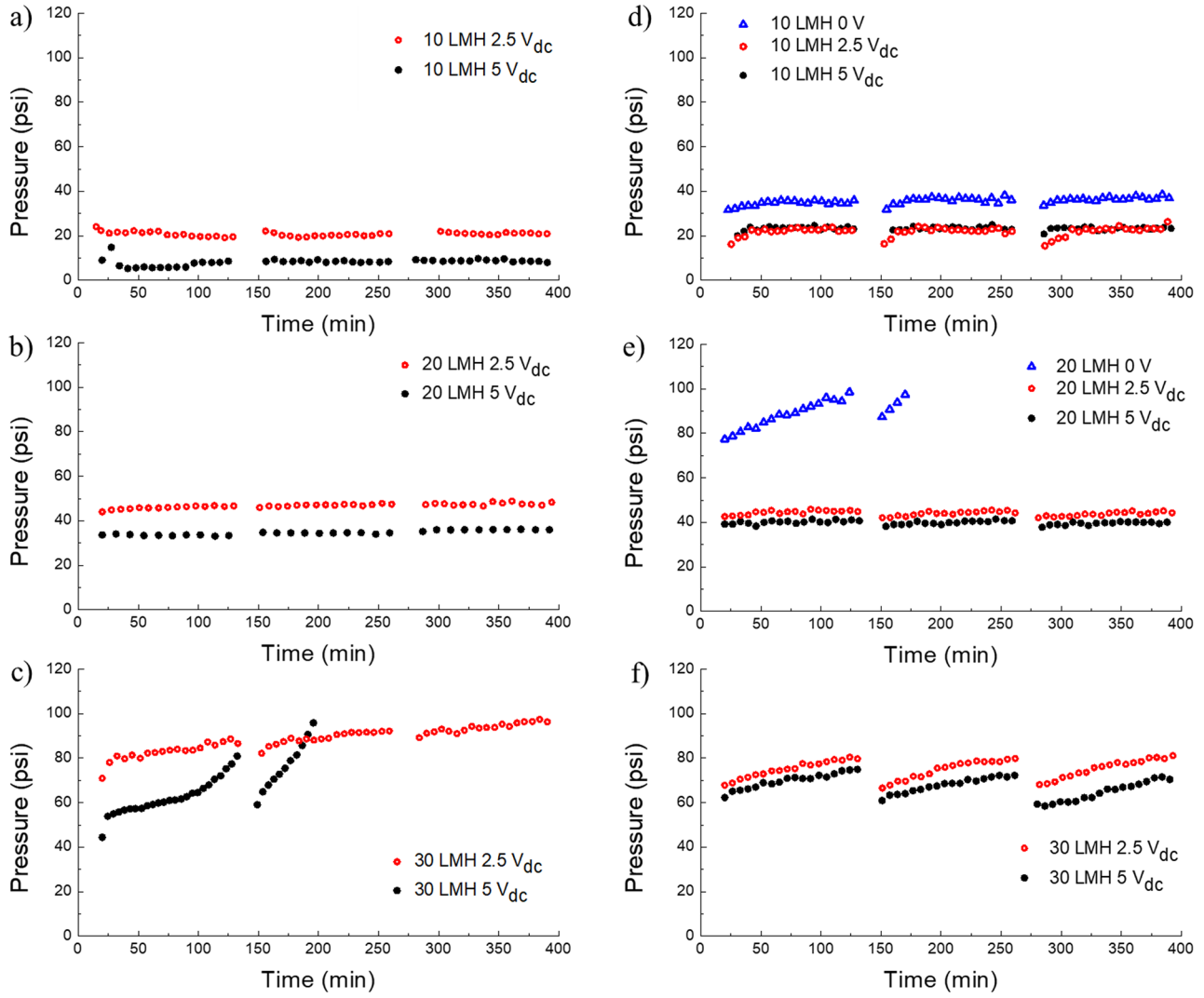

Figure 2. Membrane filtration under different ionic strengths and electrical conditions. Membranes were back-flushed every 2 h, as indicated by the break between symbols. Membranes were charged with 0, 2.5 V_{dc}, 5 V_{dc}, or 2.5 V_{ac} and system was operated at fluxes (a) 10, (b) 20, and (c) 30 LMH in 0 mM NaCl. (d), (e), and (f) represent the system being operated under the same conditions except the solution was changed to 100 Mm NaCl.

Figure 1e,f. PES-CNT membranes are readily wetted by DDBS stabilized oil emulsion in DI water, with a contact angle of 35.1 ± 3.5 degree (Figure 1e). The contact angle dramatically increased to 163.2 ± 1.7 degree when the solution was changed to 100 mM NaCl (Figure 1f). This dramatic shift is likely a result of the increased surfactant concentration at the oil/water interface, which forms a more robust layer between the membrane and oil and reduces the likelihood of the oil coming into direct contact with the membrane surface itself. This conclusion is further supported by interfacial tension measurements in the presence and absence of the electrolyte. The interfacial tensions of droplets in 0 mM NaCl and 100 mM NaCl solution were measured using the pendant drop method. In DI water, the oil/water interfacial tension was determined to be 22.8 ± 3.5 mN/m (Figure 1g); however, in the presence of 100 mM NaCl, the interfacial tension dropped by a factor of 10 to 2.0 ± 0.6 mN/m (Figure 1h). This drop in interfacial tension is associated with the higher packing of surfactant molecules at the oil/water interface enabled by the reduced electrostatic repulsion between the charged groups of the hydrophilic surfactant heads.

3.3. Membrane Filtration Results. Oil emulsions in DI water or in 100 mM NaCl were filtrated using PES-CNT membranes at 10, 20, and 30 LMH, under different applied electrical potentials (Figure 2); Membrane surface potentials versus a Ag/AgCl reference at 2.5 V_{dc} and 5 V_{dc} cell potentials were determined using the open circuit potential method,[29] with potentials of −1,000 mV and −2,300 mV in DI water, and −1300 mV and −3400 mV in 100 mM NaCl, under 2.5 V_{dc} and 5 V_{dc} conditions, respectively (SI Figure S1). While we did not observe any bubble formation (caused by water electrolysis on the membrane), we cannot completely rule out their formation and/or participation in the observed fouling phenomena. When filtering emulsions in DI water, PES-CNT membranes experienced instant fouling at 0 V (data not shown). This indicates that intrinsic membrane properties such as surface hydrophobicity leads to rapid membrane wetting, which obstructs the flow of water. The application of 2.5 V_{dc} and 5 V_{dc} reduced membrane fouling, allowing the filtration process to run continuously, with no fouling observed, at 10 LMH (Figure 2a). A similar trend was observed in a study by Zhang & Vecitis, where they conclude that a potential-induced change in the concentration polarization layer is responsible for the observed antifouling phenomena.[48] Interestingly, the pressure required to maintain a flux of 10 LMH was dependent on

DOI: 10.1021/acs.est.8b02578
Environ. Sci. Technol. 2018, 52, 11591−11600

the applied potential. When 2.5 V_{dc} were applied, the required pressure was 18 ± 3 psi, whereas when 5 V_{dc} were applied, the required pressure was 10 ± 2 psi. The lower initial pressure requirements at higher potentials (5 V_{dc} vs 2.5 V_{dc}) may be caused by capacitance-induced hydrophilicity, which results in lower hydraulic resistance. These results indicate that under low ionic strength conditions, the induced electrostatic repulsive forces between the membrane and the emulsified oil drops (both negatively charged) are capable of repelling the oil drops from the membrane surface, which prevented membrane fouling.

When the flux was increased to 20 LMH, membrane fouling was very mild under both applied potentials (Figure 2b). Under these conditions, hydraulic pressure gradually increased from 44 to 48 psi, and from 33 to 36 psi after running three cycles under 2.5 V_{dc} and 5 V_{dc}, respectively. Importantly, the fouling, while mild, was not reversible, with the hydraulic cleaning steps (backwashing and cross-flow washing) not capable of restoring flux. Once again, the higher applied potential resulted in lower pressures needed to maintain the flux. When flux increased to 30 LMH, pressure requirements rose sharply (from 80 to 95 psi, and from 55 to 100 psi under 2.5 V_{dc} and 5 V_{dc}, respectively), indicating that sever fouling occurred (Figure 2c). Again, hydraulic cleaning was not capable of recovering the membrane's flux.

When treating emulsions in 100 mM NaCl solution, both AC potentials and DC potentials were investigated; here, AC conditions were tested with the goal of inducing dielectrophoresis, which may prevent oil drops from accumulating on the membrane surface. DC potentials where the membrane serves as an anode were not studied because of the probable occurrence of CNT electro-oxidation.[44] As shown in Figure 2d and SI Figure S4a, applying 2.5 V_{ac} potentials at 1 and 10 Hz accelerated membrane fouling at 10 LMH, while DC potentials at 0 V, 2.5 V_{dc} and 5 V_{dc} did not foul membranes, with the required pressure remaining constant throughout the experiment. These results indicate that dielectrophoresis does not contribute to fouling prevention, but negative potentials were able to prevent fouling. When oil drops stabilized with the positively charged CTAB surfactant were treated at 10 LMH at 2.5 V_{dc}, the membranes experienced a rapid increase in pressure (SI Figure S4b). This result shows that electrostatic attractive forces between the negatively charged membrane and the positively charged emulsified oil drops contribute to rapid membrane fouling. Furthermore, as in the DI water conditions, the application of a negative potential to the membrane surface resulted in lower pressures needed to maintain flux. When the flux was increased to 20 LMH, membranes were irreversibly fouled by oil droplets under 0 V, with pressure increasing rapidly from 65 to 100 psi (Figure 2e). However, the system pressure remained steady (i.e., no fouling was observed) when 2.5 V_{dc} and 5 V_{dc} were applied to the membrane surface, with pressures being slightly lower under the 5 V_{dc} conditions (Figure 2e). At 30 LMH, membrane fouling became more significant, resulting in a pressure increase from 68 to 80 psi (2.5 V_{dc}) and 60−75 psi (5 V_{dc}) within each cycle (Figure 2f). Interestingly, membrane fouling was reversible at this high ionic strength, and the flux could be restored using hydraulic cleaning.

The additional energy associated with the application of electrical potentials to the membrane surface is explored in the SI (SI 12). The energy was estimated to be 0.08 kWh/m^3 and 0.42 kWh/m^3 at 2.5 and 5 V, respectively, in 100 mM NaCl, and 0.008 kWh/m^3 and 0.10 kWh/m^3 for 2.5 and 5 V, respectively, in 0 M NaCl; these calculations assume a flux of 30 LMH.

3.4. Membrane Permeate Quality. TOC concentrations (a measure of water quality and oil rejection) were measured in the membrane permeate as a function of the applied electrical conditions and ionic strength (SI Figure S3). In DI water under 0 V, the membrane fouled instantly and no permeate could be collected. When 2.5 V_{dc} and 5 V_{dc} were applied to the membrane surface, TOC values of 32 ± 13 and 21 ± 4 ppm were measured (99.3% and 99.5% removal), respectively. TOC concentrations in permeate generated from emulsions in 100 mM NaCl, were higher: 73 ± 12 and 30 ± 5 ppm under 2.5 V_{dc} and 5 V_{dc} (98.3% and 99.3% removal), respectively. Under 0 and 2.5 V_{ac} conditions, the permeate showed higher TOC values of 170 ± 30, and 115 ± 45 ppm (96.1% and 97.3% removal), respectively. Not surprisingly, the applied negative electrical potentials behaved as a barrier that repelled both droplets and surfactants, reducing TOC values in the permeate.[49] Using the formation of the ionic pair between methylene blue and the anionic surfactant,[43] the concentrations of surfactant in the permeate were determined to be fairly independent of the ionic strength and electrical conditions, ranging between 10 and 18 ppm (SI Figure S3). Thus, majority of the TOC measured in the permeate was likely contributed by oil penetrating through the membrane. Based on our calculations, an average-sized oil droplet in our system (2.2 μm in diameter) would require a minimum pressure of 554 psi to deform and penetrate through the membrane's pores, which is dramatically greater than the operating pressures in our system (SI Section SI 10).[31] However, the critical pressure needed to deform oil drops declines with their size. Thus, it is likely that smaller droplets could deform and penetrate the membrane. In addition, it is likely that the application of an electrical potential increases the rejection of these small oil droplets, which results in the overall lower TOC levels measured in the permeate upon the application of cathodic potentials (SI Figure S3).

3.5. Force Analysis for Droplets near Membrane Surface. To understand the mechanism behind the observed antifouling phenomena, we conducted an overall force analysis on emulsified oil drops along the membrane surface. In our filtration system, the membranes were facing down, which caused the buoyancy force to push the oil drops against the membrane surface, as illustrated in Figure 3. The total attractive

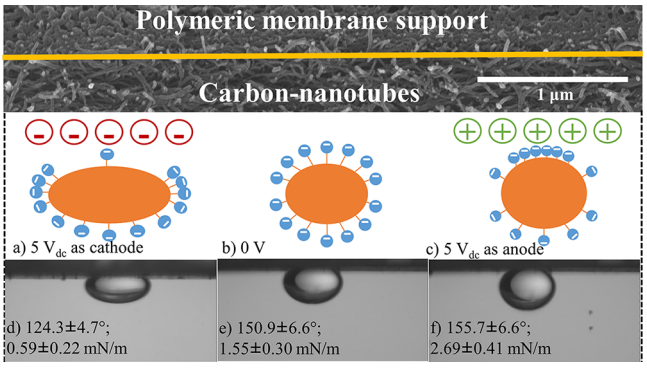

Figure 3. Proposed surfactant redistribution at (a) 5 V_{dc} with membrane as cathode, (b) 0 V, and (c) 5 V_{dc} with membrane as anode; Droplet contact angle and interfacial tension in 100 mM NaCl in response to the applied electrical potential (d−f).

force between the membrane and the oil droplet is a sum of the permeate drag force (F_d), the buoyance force (F_b), and

DOI: 10.1021/acs.est.8b02578
Environ. Sci. Technol. 2018, 52, 11591−11600

the short-range Van der Waal force (F_{vdw}). The repulsive force (keeping the oil away from the membrane) is the sum of the cross-flow lifting force (F_l) and the electrostatic repulsive force (F_{es}). The detailed equations used to calculate these specific forces are listed in the SI (SI 6). Based on our calculation, F_b gives a net attractive force of 10^{-5} nN; the repulsive lift force, F_l, has a value of 10^{-5} nN. These forces are independent of the distance from the membrane surface. At close ranges to the membrane surface (less than 100 nm), the magnitude of these forces was significantly smaller than the other forces in the system (F_d is larger than 10^{-3} nN at 100 nm and larger than 10^{-2} nN at 50 nm). The magnitude of the drag forces experienced by an oil drop are impacted by water flux (10, 20, or 30 LMH). However, these differences are not dramatic, with F_d values of 3×10^{-2}, 5×10^{-2}, and 8×10^{-2} nN for a flux of 10, 20, and 30 LMH at a distance of 5 nm, respectively (SI Figure S4). The overall force curves at all fluxes are presented in SI Figure S5. In these curves, positive values represent repulsive forces between the oil droplet and the membrane surface, while negative values represent attractive forces. We assumed a membrane surface potential of −100 mV when no electrical potential was applied, with the negative potential attributed to surface hydroxyl and carboxylic groups on the CNTs.[36,50] Our modeling results indicate that using the membrane as a cathode can significantly enhance the maximum repulsive force in DI water; for example, at 20 LMH the maximum force increased from 2 nN at −100 mV to 21 nN at −1000 mV (SI Figure S5b). Increasing the applied potentials (to −2300 mV) did not dramatically increase the repulsing force (maximum of 21 nN), although the distance from the surface where the maximum repulsive force occurs extended further away from the membrane (from 5.3 nm at −1,000 mV to 6.7 nm at −2300 mV). This is not surprising, as the maximum repulsive force is a function of the maximum ionic concentration in the electrical double layer (EDL), with the concentrations reaching saturation at these high potentials.[36] Therefore, increasing the potential from 2.5 V_{dc} to 5 V_{dc} simply increases the thickness of this saturated layer, pushing the point of maximum repulsive force away from the surface. When the ionic strength was increased to 100 mM, our calculations showed that the maximum repulsive force declined relative to the DI water case (SI Figure S5d−f). Here, the maximum repulsive force was calculated to be 9 nN, 10 nN, and 10 nN for surface potentials of −100 mV, −1,300 mV, and −3,400 mV, respectively (at 20 LMH, SI Figure S5e). This is caused by the increased ionic strength of the bulk solution, which results in a smaller difference between the concentration in the bulk and the EDL, and consequently to a smaller difference in osmotic pressure between the bulk solution and the space between the membrane and oil drop. At 20 LMH, the distance where the maximum repulsion occurred increased from 3.6 nm (at −100 mV) to 5.2 nm (at −1,300 mV), to 6.3 nm (at −3,400 mV). Our model also indicates the presence of a very shallow secondary repulsive peak at approximately 17 nm, although it is unclear whether this shallow peak has any real significance. While the force models are quite similar across all fluxes, our experiments show rapid fouling at 30 LMH under all conditions (Figure 2c,f). Thus, we speculate that an additional mechanism/s are responsible for the observed fouling (i.e., other droplet/membrane and droplet/droplet processes are taking place, which are not accounted for by the force balance described above).

3.6. Proposed Mechanisms of Reduced Membrane Fouling. The impact of the applied electrical potential on the shape, contact angle, and interfacial tension of emulsified oil droplets at the membrane/water interface can be seen in Figure 3. The shape of the drop changed dramatically as a function of the applied potential. When the membrane was used as a cathode, the oil drop assumed a more oblong shape, compared to the 0 V case (Figure 3d and e). However, when the membrane was used as an anode, the oil drop became more circular (Figure 3f). The shape of an oil drop can be used to calculate the interfacial tension of the drop.[51] Based on drop-shape image analysis, we determined that the interfacial tension was 1.55 ± 0.30 mN/m at 0 V, decreasing to 0.80 ± 0.11 and 0.59 ± 0.22 mN/m under cathodic 2.5 and 5 V conditions, and increasing to 2.69 ± 0.41 mN/m under anodic conditions (Figures 3d−f). The applied potential also resulted in a change in the contact angle of the oil drop, with a contact angle of 150.9 ± 6.6° at 0 V, decreasing to 135.0 ± 4.0 and 124.3 ± 4.7° with a cathodic membrane (2.5 and 5 V_{dc}), and increasing to 155.7 ± 6.7° with an anodic membrane (Figures 3d−f). We propose that these changes are caused as a result of a change in the surfactant distribution at the oil/water interface in response to the applied potential. We confirmed this interfacial tension (oil/membrane interface) change using our experimental contact angle data in SI Section 1.5 (used to model surface wetting). DDBS (used to stabilize the oil) is an anionic surfactant with a negatively charged sulfonated functional group. When the membrane was used as a cathode, the ionic heads of the surfactant were repelled from the membrane and redistributed around the oil drop (Figure 3a). As a result, fewer surfactant molecules were left at the oil/membrane interface, while more surfactant molecules were located at the oil/water interface, which would explain the lowering of the membrane/oil contact angle, and the lower oil/water interfacial tension measurement. The opposite phenomenon occurred when the membrane was used as an anode, that is, the negatively charged surfactant molecules were attracted to the membrane surface, which results in more surfactant at the membrane/oil interface (higher contact angle) and less surfactant at the oil/water interface (higher interfacial tension, and less electrostatic repulsion between neighboring droplets). Oil in water emulsions with a higher interfacial tension (at the oil/water interface) tend to coalesce more, which can lead to enhanced membrane fouling.[52]

In general, emulsions with lower contact angle will wet the membrane surface more easily, causing membrane fouling.[19] However, in our system we observed an opposite phenomenon, namely, reduced fouling under cathodic conditions. Therefore, we propose that the dominant fouling mechanism under high ionic strength conditions is due to droplet coalescence, which results in larger oil droplets, making pore blocking and membrane wetting more likely.[7,32] A schematic of our proposed fouling mechanism can be seen in Figure 4a. As can be seen, cathodic or anodic potentials lead to different surfactant distributions around oil drops along the membrane surface, which impacts their propensity to coalesce and wet the membrane. To determine the likelihood of oil drops at the membrane surface to experience coalescence under our experimental conditions, we used the film drainage model (SI 8, Table S4).[53] In this model, the coalescence frequency, λ, is defined by the drainage time, $t_{drainage}$, and contact time, $t_{contact}$ (see eq 1). The explicit expressions used to describe $t_{drainage}$ and $t_{contact}$ are listed in the SI (Section 1.6). Upon rearrangement, λ can be expressed as a function of the interfacial tension,, and a positive constant (C) (eq 1). Based on our calculations,

DOI: 10.1021/acs.est.8b02578
Environ. Sci. Technol. 2018, 52, 11591−11600

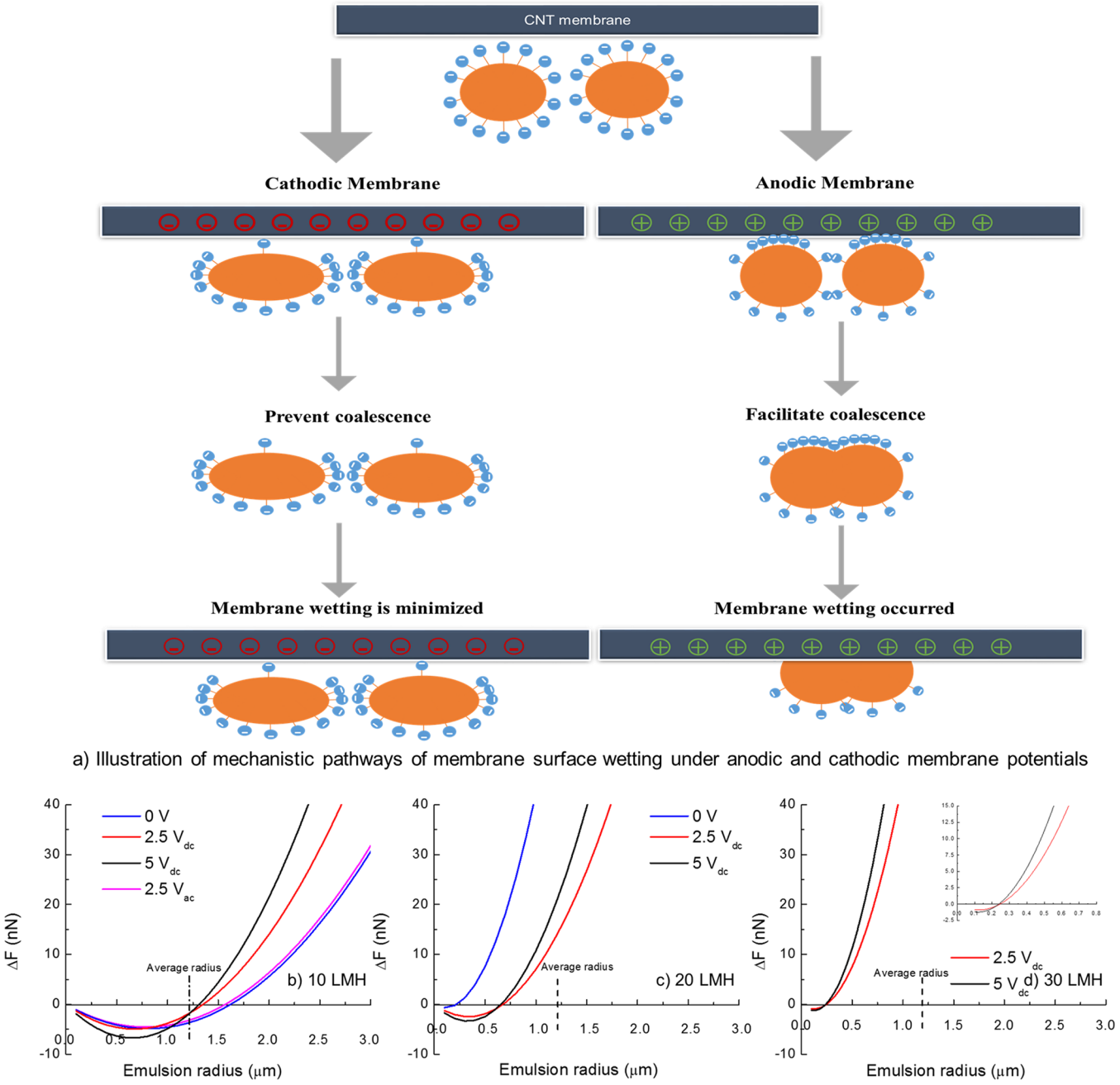

Figure 4. (a) Illustration of mechanistic pathways of membrane surface wetting under anodic and cathodic membrane potentials. Impact of droplet size on membrane surface wetting under (b) 10 LMH, (c) 20 LMH and (d) 30 LMH;.

λ decreases from 0.19 ± 0.04 at 0 V to 0.04 ± 0.02 at 2.5 V_{dc}, and 0.02 ± 0.01 at 5 V_{dc} in 100 mM NaCl. Under anodic 5 V condition, λ increased to 0.38 ± 0.02. Therefore, negative membrane potentials reduced the probability of droplet coalescence.

$$\lambda = \exp\left(-\frac{t_{drainage}}{t_{contact}}\right) \sim \exp(-C\gamma^{-1}) \quad (1)$$

To estimate the relationship between the increased droplet size (from coalescence) and membrane wetting, we made some highly simplifying assumptions. Specifically, we assumed that when oil drops accumulate in the cake layer, they do not deform, instead acting as solid spheres that are in direct contact with each other. In fact, for droplet coalescence to occur, oil drops must first come in direct contact with each other (i.e., film drainage must occur). Thus, we believe these assumptions are supported by our experimental findings. We use these assumptions to calculate specific values for the different forces occurring at the membrane/oil interface; importantly, while these assumptions ignore certain droplet properties, we believe our results are relevant in terms of trends, if not necessarily in terms of absolute values.

The accumulation of oil drops at the membrane surface forms a cake-layer, which results in a pressure drop across the layer; this pressure-drop was determined from the increase in pressure during the first cycle (Figures 2d–f) and used to calculate the compressive force ($F_{\Delta p}$) acting on an oil drop at the membrane/water interface (SI SI 9; Table S5).[31,54] We defined ΔF as the difference between $F_{\Delta p}$ and the surface

DOI: 10.1021/acs.est.8b02578
Environ. Sci. Technol. 2018, 52, 11591−11600

force resisting membrane oil wetting (F_{wr}; SI eqs S25−S27). The magnitude of ΔF is highly dependent on the droplet size, with larger drops leading to more wetting (SI eq S28). A positive ΔF value indicates membrane wetting will occur. ΔF values were plotted as a function of the droplet size (Figure 4b−d). At 10 LMH, ΔF is negative for droplet sizes smaller than the average droplet size (a radius of 1.1 μm in 100 mM NaCl), regardless of applied electrical potentials (Figure 4b). However, under the 2.5 Vac condition, droplets have a higher probability of coalescence ($\lambda = 0.38 \pm 0.02$). We speculate that under these conditions, droplets will coalesce, with their radius increasing beyond the size where ΔF becomes positive when (radius >1.6 μm), resulting in membrane wetting (Figure 2d, Figure 4b). When flux was increased to 20 LMH, no significant fouling was observed under the 2.5 V_{dc} and 5 V_{dc} conditions, but the membrane rapidly fouled at 0 V (Figure 2e). In the case of 0 V, the model predicts wetting when droplets are larger than 0.2 μm (Figure 4c). In contrast, the model predicted positive ΔF values for droplets >0.6 μm under the 2.5 V_{dc} and 5 V_{dc} conditions (Figure 4c). Under the 0 V conditions, some coalescence is likely taking place ($\lambda = 0.19 \pm 0.04$), which would grow the droplet drops, and facilitate wetting. Under 2.5 V_{dc} and 5 V_{dc} λ decreases to 0.04 ± 0.02 and 0.02 ± 0.01, respectively, which would limit coalescence. It is known that small particles (droplets) are preferentially deposited on rough surfaces, such as our membrane.[55,56] Thus, considering the droplet size distribution, and the very low coalescence probability, it is possible that the fouling layer is composed of noncoalescing drops with sizes <0.6 μm, which do not wet the membrane, and do not lead to irreversible fouling. When the flux increased to 30 LMH, no irreversible fouling was observed under 2.5 V_{dc} and 5 V_{dc} conditions (Figure 2f), indicating that no membrane wetting occurred. Again, we reason that this is caused by the dominance of small oil drops in the cake layer (<0.25 μm) and the lack of coalescence events (Figure 4d). Interestingly, the model predicts larger ΔF values under 5 V_{dc} conditions, compared to 2.5 V_{dc} when the droplet size exceeds the critical threshold (Figure 4b-d). This is likely caused by the higher interfacial tension (oil/membrane interface) and lower contact angles at the higher potential induced by the enhanced redistribution of surfactants (SI Section 1.5).

■ ASSOCIATED CONTENT

Supporting Information

The Supporting Information is available free of charge on the ACS Publications website at DOI: 10.1021/acs.est.8b02578.

Detailed information on emulsion size distribution (Table S1); membrane surface open potential (Figure S1); surfactant surface density (Table S2); the correlation between the interfacial tension and surfactant concentration (Figure S2); membrane permeate quality (Figure S3); additional membrane filtration results for 2.5Vac at 1 and 10 Hz, and cationic surfactant stabilized droplets (Figure S4); force calculation and combined force curves (Table S3, Figure S5); emulsion interfacial tension calculation (oil/membrane interface) (Figure S6); coalescence probability calculation (Table S4); membrane surface wetting (Table S5); a summary of previous studies using membrane treating oily wastewater (Table S6); energy and cost analysis (SI 12) (PDF)

■ AUTHOR INFORMATION

Corresponding Author

*Phone: 310-825-1346; e-mail: jassby@ucla.edu.

ORCID

Guy Z. Ramon: 0000-0002-0711-0654

David Jassby: 0000-0002-2133-2536

Notes

The authors declare no competing financial interest.

■ ACKNOWLEDGMENTS

This work was generously supported by the Office of Naval Research under award number N00014-14-1-0809, and the National Science Foundation under award number 1553756.

■ REFERENCES

(1) Zhong, J.; Sun, X.; Wang, C. Treatment of Oily Wastewater Produced from Refinery Processes Using Flocculation and Ceramic Membrane Filtration. *Sep. Purif. Technol.* **2003**, *32* (1−3), 93−98.

(2) Peng, H.; Tremblay, A. Y. Membrane Regeneration and Filtration Modeling in Treating Oily Wastewaters. *J. Membr. Sci.* **2008**, *324* (1−2), 59−66.

(3) Ghidossi, R.; Veyret, D.; Scotto, J. L.; Jalabert, T.; Moulin, P. Ferry Oily Wastewater Treatment. *Sep. Purif. Technol.* **2009**, *64*, 296−303.

(4) Tomaszewska, M.; Orecki, A.; Karakulski, K. Treatment of Bilge Water Using a Combination of Ultrafiltration and Reverse Osmosis. *Desalination* **2005**, *185* (1−3), 203−212.

(5) Mueller, J.; Cen, Y.; Davis, R. H. Crossflow Microfiltration of Oily Water. *J. Membr. Sci.* **1997**, *129* (2), 221−235.

(6) Neff, J.; Lee, K.; Deblois, E. M. *Produced Water : Overview of Composition, Fates, and Effects*; Springer Science+Business Media, 2011.

(7) Dickhout, J. M.; Moreno, J.; Biesheuvel, P. M.; Boels, L.; Lammertink, R. G. H.; de Vos, W. M. Produced Water Treatment by Membranes: A Review from a Colloidal Perspective. *J. Colloid Interface Sci.* **2017**, *487*, 523−534.

(8) Kemp, J. *Waste Water: America's Hidden 60 Million Barrel A Day Industry* https://www.huffingtonpost.com/2012/01/16/waste-water-barrel_n_1208587.html.

(9) *Produced Water Beneficial Use Case Studies*, http://aqwatec.mines.edu/produced_water/assessbu/case/.

(10) Johnston, C.. *EPA Regulation of Discharges to Surface Waters*; IPEC: Houston, 2007.

(11) Gryta, M.; Karakulski, K.; Morawski, A. W. Purification of Oily Wastewater by Hybrid UF/MD. *Water Res.* **2001**, *35* (15), 3665−3669.

(12) Fakhru'l-Razi, A.; Pendashteh, A.; Abdullah, L. C.; Biak, D. R. A.; Madaeni, S. S.; Abidin, Z. Z. Review of Technologies for Oil and Gas Produced Water Treatment. *J. Hazard. Mater.* **2009**, *170* (2−3), 530−551.

(13) Seals, S. T. *Phase I Final Rule and Technical Development Document of Uniform National Discharge Standards (UNDS) Stern Tube Seals and Underwater Bearing Lubrication : Nature of Discharge.* 1999, No. April.

(14) Chakrabarty, B.; Ghoshal, A. K.; Purkait, M. K. Ultrafiltration of Stable Oil-in-Water Emulsion by Polysulfone Membrane. *J. Membr. Sci.* **2008**, *325* (1), 427−437.

(15) Kong, J.; Li, K. Oil Removal from Oil-in-Water Emulsions Using PVDF Membranes. *Sep. Purif. Technol.* **1999**, *16* (1), 83−93.

(16) Han, G.; de Wit, J. S.; Chung, T. S. Water Reclamation from Emulsified Oily Wastewater via Effective Forward Osmosis Hollow Fiber Membranes under the PRO Mode. *Water Res.* **2015**, *81*, 54−63.

(17) Duong, P. H. H.; Chung, T. S. Application of Thin Film Composite Membranes with Forward Osmosis Technology for the Separation of Emulsified Oil-Water. *J. Membr. Sci.* **2014**, *452*, 117−126.

DOI: 10.1021/acs.est.8b02578
Environ. Sci. Technol. 2018, 52, 11591−11600

(18) Alkhudhiri, A.; Darwish, N.; Hilal, N. Produced Water Treatment: Application of Air Gap Membrane Distillation. *Desalination* **2013**, *309*, 46−51.
(19) Wang, Z.; Lin, S. Membrane Fouling and Wetting in Membrane Distillation and Their Mitigation by Novel Membranes with Special Wettability. *Water Res.* **2017**, *112*, 38−47.
(20) Huang, Y. X.; Wang, Z.; Jin, J.; Lin, S. Novel Janus Membrane for Membrane Distillation with Simultaneous Fouling and Wetting Resistance. *Environ. Sci. Technol.* **2017**, *51* (22), 13304−13310.
(21) Hou, D.; Wang, Z.; Wang, K.; Wang, J.; Lin, S. Composite Membrane with Electrospun Multiscale-Textured Surface for Robust Oil-Fouling Resistance in Membrane Distillation. *J. Membr. Sci.* **2018**, *546* (September2017), 179−187.
(22) Zhang, S.; Lu, F.; Tao, L.; Liu, N.; Gao, C.; Feng, L.; Wei, Y. Bio-Inspired Anti-Oil-Fouling Chitosan-Coated Mesh for Oil/Water Separation Suitable for Broad Ph Range and Hyper-Saline Environments. *ACS Appl. Mater. Interfaces* **2013**, *5* (22), 11971−11976.
(23) Zhou, X.; He, C. Tailoring the Surface Chemistry and Morphology of Glass Fiber Membranes for Robust Oil/Water Separation Using Poly(Dimethylsiloxanes) as Hydrophobic Molecular Binders. *J. Mater. Chem. A* **2018**, *00*, 1−9.
(24) Tummons, E. N.; Tarabara, V. V.; Chew, J. W.; Fane, A. G. Behavior of Oil Droplets at the Membrane Surface during Crossflow Microfiltration of Oil-Water Emulsions. *J. Membr. Sci.* **2016**, *500*, 211−224.
(25) Padaki, M.; Surya Murali, R.; Abdullah, M. S.; Misdan, N.; Moslehyani, A.; Kassim, M. A.; Hilal, N.; Ismail, A. F. Membrane Technology Enhancement in Oil-Water Separation. A Review. *Desalination* **2015**, *357*, 197−207.
(26) Matsumoto, Y.; Kawakatsu, T.; Nakajima, M.; Kikuchi, Y. Visualization of Filtration Phenomena of a Suspended Solution Including O/W Emulsion or Solid Particle and Membrane Separation Properties of the Solution. *Water Res.* **1999**, *33* (4), 929−936.
(27) Zhu, L.; Chen, M.; Dong, Y.; Tang, C. Y.; Huang, A.; Li, L. A Low-Cost Mullite-Titania Composite Ceramic Hollow Fiber Microfiltration Membrane for Highly Efficient Separation of Oil-in-Water Emulsion. *Water Res.* **2016**, *90*, 277−285.
(28) Norouzbahari, S.; Roostaazad, R.; Hesampour, M. Crude Oil Desalter Effluent Treatment by a Hybrid UF/RO Membrane Separation Process. *Desalination* **2009**, *238*, 174−182.
(29) Lee, H.; Yoon, S. W.; Kim, E. J.; Park, J. In-Situ Growth of Copper Sulfide Nanocrystals on Multiwalled Carbon Nanotubes and Their Application as Novel Solar Cell and Amperometric Glucose Sensor Materials. *Nano Lett.* **2007**, *7* (3), 778−784.
(30) Zhang, Q.; Arribas, P.; Remillard, E. M.; García-Payo, M. C.; Khayet, M.; Vecitis, C. D. Interlaced CNT Electrodes for Bacterial Fouling Reduction of Microfiltration Membranes. *Environ. Sci. Technol.* **2017**, *51* (16), 9176−9183.
(31) Zhu, X.; Dudchenko, A.; Gu, X.; Jassby, D. Surfactant-Stabilized Oil Separation from Water Using Ultrafiltration and Nanofiltration. *J. Membr. Sci.* **2017**, *529* (December 2016), 159−169.
(32) Fux, G.; Ramon, G. Z. Microscale Dynamics of Oil Droplets at a Membrane Surface: Deformation, Reversibility, and Implications for Fouling. *Environ. Sci. Technol.* **2017**, *51* (23), 13842−13849.
(33) Gragson, D. E.; Richmond, G. L. Investigations of the Structure and Hydrogen Bonding of Water Molecules at Liquid Surfaces by Vibrational Sum Frequency Spectroscopy. *J. Phys. Chem. B* **1998**, *102* (20), 3847−3861.
(34) Santos, F. K. G.; Neto, E. L. B.; Moura, M. C. P. A.; Dantas, T. N. C.; Neto, A. A. D. Molecular Behavior of Ionic and Nonionic Surfactants in Saline Medium. *Colloids Surf., A* **2009**, *333* (1−3), 156−162.
(35) Gurkov, T. D.; Dimitrova, D. T.; Marinova, K. G.; Bilke-Crause, C.; Gerber, C.; Ivanov, I. B. Ionic Surfactants on Fluid Interfaces: Determination of the Adsorption; Role of the Salt and the Type of the Hydrophobic Phase. *Colloids Surf., A* **2005**, *261* (1−3), 29−38.
(36) Dudchenko, A. V.; Rolf, J.; Russell, K.; Duan, W.; Jassby, D. Organic Fouling Inhibition on Electrically Conducting Carbon Nanotube − Polyvinyl Alcohol Composite Ultra Filtration Membranes. *J. Membr. Sci.* **2014**, *468*, 1−10.
(37) Duan, W.; Ronen, A.; de Leon, J. V.; Dudchenko, A.; Yao, S.; Corbala-Delgado, J.; Yan, A.; Matsumoto, M.; Jassby, D. Treating Anaerobic Sequencing Batch Reactor Effluent with Electrically Conducting Ultrafiltration and Nanofiltration Membranes for Fouling Control. *J. Membr. Sci.* **2016**, *504*, 104−112.
(38) Ronen, A.; Duan, W.; Wheeldon, I.; Walker, S.; Jassby, D. Microbial Attachment Inhibition through Low-Voltage Electrochemical Reactions on Electrically Conducting Membranes. *Environ. Sci. Technol.* **2015**, *49* (21), 12741−12750.
(39) De Lannoy, C. F.; Jassby, D.; Gloe, K.; Gordon, A. D.; Wiesner, M. R. Aquatic Biofouling Prevention by Electrically Charged Nanocomposite Polymer Thin Film Membranes. *Environ. Sci. Technol.* **2013**, *47* (6), 2760−2768.
(40) Tang, L.; Iddya, A.; Zhu, X.; Dudchenko, A. V.; Duan, W.; Turchi, C.; Vanneste, J.; Cath, T. Y.; Jassby, D. Enhanced Flux and Electrochemical Cleaning of Silicate Scaling on Carbon Nanotube-Coated Membrane Distillation Membranes Treating Geothermal Brines. *ACS Appl. Mater. Interfaces* **2017**, *9* (44), 38594−38605.
(41) Duan, W.; Dudchenko, A.; Mende, E.; Flyer, C.; Zhu, X.; Jassby, D. Electrochemical Mineral Scale Prevention and Removal on Electrically Conducting Carbon Nanotube-Polyamide Reverse Osmosis Membranes. *Environ. Sci. Process. Impacts* **2014**, *16* (6), 1300−1308.
(42) Slade, A.; Jassby, D.; Hilal, N.; Al-Zoubi, H.; Darwish, N.; Mohamma, A.; Arabi, M. A.; Pendergast, M. M.; Hoek, E. M.; Sobsey, M. D.; et al. Affordable, Flexible, and Modular: A Guide to Open-Source Membrane-Based Water Treatment Systems. *Environ. Sci. Water Res. Technol.* **2016**, *2* (6), 965−974.
(43) Jurado, E.; Fernández-Serrano, M.; Núñez-Olea, J.; Luzón, G.; Lechuga, M. Simplified Spectrophotometric Method Using Methylene Blue for Determining Anionic Surfactants: Applications to the Study of Primary Biodegradation in Aerobic Screening Tests. *Chemosphere* **2006**, *65* (2), 278−285.
(44) Duan, W.; Ronen, A.; Walker, S.; Jassby, D. Polyaniline-Coated Carbon Nanotube Ultrafiltration Membranes: Enhanced Anodic Stability for in Situ Cleaning and Electro-Oxidation Processes. *ACS Appl. Mater. Interfaces* **2016**, *8* (34), 22574−22584.
(45) Para, G.; Jarek, E.; Warszynski, P. The Surface Tension of Aqueous Solutions of Cetyltrimethylammonium Cationic Surfactants in Presence of Bromide and Chloride Counterions. *Colloids Surf., A* **2005**, *261* (1−3), 65−73.
(46) Ghosh, P.; Banik, M. Effects of Salts Containing Mono-, Di-, and Trivalent Ions on Electrical and Rheological Properties of Oil-Water Interface in Presence of Cationic Surfactant: Importance in the Stability of Oil-in-Water Emulsions. *J. Dispersion Sci. Technol.* **2014**, *35* (4), 471−481.
(47) Mabille, C.; Schmitt, V.; Gorria, P.; Leal Calderon, F.; Faye, V.; Deminière, B.; Bibette, J. Rheological and Shearing Conditions for the Preparation of Monodisperse Emulsions. *Langmuir* **2000**, *16* (2), 422−429.
(48) Zhang, Q.; Vecitis, C. D. Conductive CNT-PVDF Membrane for Capacitive Organic Fouling Reduction. *J. Membr. Sci.* **2014**, *459*, 143−156.
(49) Yi, G.; Chen, S.; Quan, X.; Wei, G.; Fan, X.; Yu, H. Enhanced Separation Performance of Carbon Nanotube−polyvinyl Alcohol Composite Membranes for Emulsified Oily Wastewater Treatment under Electrical Assistance. *Sep. Purif. Technol.* **2018**, *197* (December 2017), 107−115.
(50) Kang, S. T.; Subramani, A.; Hoek, E. M. V.; Deshusses, M. A.; Matsumoto, M. R. Direct Observation of Biofouling in Cross-Flow Microfiltration: Mechanisms of Deposition and Release. *J. Membr. Sci.* **2004**, *244* (1−2), 151−165.
(51) Kingery, W. D.; Humenik, M. Surface Tension. At Elevated Temperatures. I. Furnace and Method for Use of the Sessile Drop Method; Surface Tension of Silicon, Iron and Nickel. *J. Phys. Chem.* **1953**, *57* (3), 359−363.

DOI: 10.1021/acs.est.8b02578
Environ. Sci. Technol. 2018, 52, 11591−11600

(52) Chesters, a. K. The modelling of coalescence process in fluid-liquid dispersions: A review of current understanding. *Chem. Eng. Res. Des.* **1991**, *69* (4), 259−270.
(53) Liao, Y.; Lucas, D. A Literature Review on Mechanisms and Models for the Coalescence Process of Fluid Particles. *Chem. Eng. Sci.* **2010**, *65* (10), 2851−2864.
(54) Yoon, S.-H.; Forsgren, A. J.; Walker, H. W. *Membrane Bioreactor Processes: Principles and Applications*; CRC Press, 2015.
(55) Li, X.; Zhang, P.; Lin, C. L.; Johnson, W. P. Role of Hydrodynamic Drag on Microsphere Deposition and Re-Entrainment in Porous Media under Unfavorable Conditions. *Environ. Sci. Technol.* **2005**, *39* (11), 4012−4020.
(56) Wiesner, M. R.; Bottero, J.-Y. *Environmental Nanotechnology Applications and Impacts of Nanomaterials*; McGraw-Hill: New York, NY, 2007.

DOI: 10.1021/acs.est.8b02578
Environ. Sci. Technol. 2018, 52, 11591−11600